

Efficient Coating Materials for Magnetite Nanoparticles

Efficient Coating Materials for Magnetite Nanoparticles

By

Noorashikin Md Saleh, Tanusha Devi,
Nik Nur Atiqah Nik Wee, Beh Shiu-an Yih,
Siti Khalijah Mahmad Rozi
and Nasuha Mohamad Nasrol

**Cambridge
Scholars
Publishing**



Efficient Coating Materials for Magnetite Nanoparticles

By Noorashikin Md Saleh, Tanusha Devi, Nik Nur Atiqah Nik Wee,
Beh Shiuan Yih, Siti Khalijah Mahmad Rozi and Nasuha Mohamad Nasrol

This book first published 2024

Cambridge Scholars Publishing

Lady Stephenson Library, Newcastle upon Tyne, NE6 2PA, UK

British Library Cataloguing in Publication Data

A catalogue record for this book is available from the British Library

Copyright © 2024 by Noorashikin Md Saleh, Tanusha Devi,
Nik Nur Atiqah Nik Wee, Beh Shiuan Yih, Siti Khalijah Mahmad Rozi
and Nasuha Mohamad Nasrol

All rights for this book reserved. No part of this book may be reproduced,
stored in a retrieval system, or transmitted, in any form or by any means,
electronic, mechanical, photocopying, recording or otherwise, without
the prior permission of the copyright owner.

ISBN: 978-1-0364-1200-5

ISBN (Ebook): 978-1-0364-1201-2

TABLE OF CONTENTS

List of Tables	x
List of Figures	xii
Acknowledgements	xvi
Abstract	xvii
List of Abbreviations	xviii
Chapter 1	Synthesis of Magnetic Nanoparticles Functionalized with Surfactant
	1
	1.1 Magnetic nanoparticles (MNPs)
	1
	1.2 Surfactants
	2
	1.2.1 Properties of surfactants
	2
	1.2.2 Types of surfactants
	2
	1.2.2.1 Anionic Surfactants
	2
	1.2.2.2 Cationic surfactants
	3
	1.2.2.3 Zwitterionic surfactants
	4
	1.2.2.4 Non-ionic surfactants
	5
	1.3 Surfactant modified magnetic nanoparticles
	5
	1.3.1 Synthesis of MNP with ferum oxide and surfactant Slygard
	6
	1.4 Characterization of MNP with ferum oxide and surfactant Sylgard
	7
	1.4.1 Morphological analysis
	8
	1.4.2 Elemental analysis
	11
	1.4.3 Functional group analysis
	13
	1.4.4 Crystallinity properties
	14
	1.4.5 Magnetic behavior
	16
	1.5 Optimization of parameters to extract pollutants in water
	17
	1.5.1 Effect of pH
	17
	1.5.2 Effects of amount of adsorbent
	19
	1.5.3 Effect of desorption solvent
	20
	1.5.4 Effect of volume of desorption solvent
	21
	1.5.5 Effect of extraction time
	22

	1.5.6 Effect of desorption time	23
	1.5.7 Effect of volume of solution	24
	1.6 Optimum conditions using response surface methodology	25
	1.6.1 Selection of lower, middle and upper levels of the design variables	25
	1.6.2 Fitting the model	26
	1.6.3 Analytical figures of merits	33
	1.7 Application on real water samples	33
Chapter 2	Synthesis of Magnetic Nanoparticles Functionalized with Amine	36
	2.1 Synthesis of amine-functionalized magnetite nanoparticles	36
	2.2 Characterization of amine-functionalized magnetite nanoparticles	39
	2.2.1 Functional group analysis	39
	2.2.2 Morphological analysis	42
	2.2.3 Elemental analysis	44
	2.3 Application of amine-functionalized magnetite nanoparticles	46
	2.4 Optimization of adsorption studies	47
	2.4.1 Effect of dosage of adsorbent	47
	2.4.2 Effect of contact time	49
	2.4.3 Effect of initial phenol concentration	50
	2.4.4 Effect of pH of phenol solution	52
	2.5 Adsorption kinetics model	53
	2.6 Adsorption isotherm models	56
	2.7 Reusability of adsorbent	58
	2.8 Comparison of amine-functionalized magnetite nanoparticles with other reported adsorbents	59

Chapter 3	Synthesis of Magnetic Nanoparticles Functionalized with Silica	61
	3.1 Biological background of silica	61
	3.2 Method of silica synthesis from rice husk	63
	3.3 Silica	64
	3.3.1 Properties of Silica	65
	3.3.2 General procedure for silica extraction	66
	3.3.2.1 Sample Preparation	66
	3.3.2.2 Alkali dissolution	67
	3.3.2.3 Deposition method	68
	3.3.2.4 Stöber's method	68
	3.3.2.5 Sol-gel method	69
	3.3.2.6 Acid nitration for the production of gel deposits	69
	3.4 Coating of silica with magnetic nanoparticles (SiO ₂ -MNP)	71
	3.5 Characterization of silica-functionalized magnetite nanoparticles	71
	3.5.1 Functional Group Analysis	71
	3.5.2 X-Ray Diffraction Analysis (XRD)	73
	3.5.3 Morphology Analysis	74
	3.5.4 Element Analysis (EDX)	77
	3.6 Optimum parameters for extraction of pollutant in water	79
	3.6.1 Effect of pH	79
	3.6.2 Effect of adsorbent weight	80
	3.6.3 Effect of sorbent type	81
	3.6.4 Volume of acetonitrile (ACN) solvent	81
	3.6.5 Extraction time	82
	3.6.6 Desorption time	83
	3.7 Mechanism interaction between magnetic silica nanoparticles with phenol in water	84

Chapter 4	Adsorption of Heavy Metal from Wastewater by Bioadsorbent <i>Modified Azolla Microphylla Lemna Minor</i>	87
	4.1 Types and Sources of Heavy Metals	87
	4.1.1 Cadmium (Cd (II))	88
	4.1.2 Copper (Cu (II))	88
	4.1.3 Zinc (Zn (II))	89
	4.2 The importance of Water to Human	89
	4.3 River Water Pollution in Malaysia	90
	4.4 Biosorbent Adsorption Techniques for Heavy Metal Detection	91
	4.4.1 Microorganism as Adsorbent	91
	4.4.2 Terminalia Catappa as Adsorbent	95
	4.4.3 Azolla as Adsorbent	97
	4.5 Methodology	99
	4.5.1 List of Chemicals	101
	4.5.2 Synthesis of <i>Azolla Microphylla Lemna Minor</i> Adsorbent	101
	4.5.3 Adsorbent Material Characterization Analysis	102
	4.5.3.1 Fourier-Transform Infrared Spectroscopy (FTIR)	103
	4.5.3.2 Scanning Electron Microscopy with Energy Dispersive X-ray Spectroscopy (SEM-EDX)	103
	4.5.3.3 'Brunanuer-Emmett-Teller' (BET)	104
	4.5.3.4 X-ray Diffraction (XRD) Analysis	105
	4.5.4 Preparation of Calibration Curve	106
	4.5.5 Optimization Parameters	106
	4.5.5.1 Contact Time	107
	4.5.5.2 Adsorbent Dose	107
	4.5.5.3 pH of the Sample Solution	107
	4.5.6 River Water Sampling	108
	4.5.7 Extraction of Heavy Metal Cu (II) In River Water	109
	4.6 Fourier Transform Infrared (FTIR) Characterization Analysis	110
	4.7 BET Characterization Analysis	112
	4.8 Scanning Electron Microscopy (SEM)	113
	4.9 Energy Dispersive X-Ray (EDX)	114

	4.10 X-Ray Diffraction (XRD) Analysis	117
	4.11 Quantitative Analysis	120
	4.12 Optimization Parameters for Adsorption of Copper in Water	122
	4.13 Method Validation of Develop Method for Extraction of Copper in Real Water	126
	4.14 Mechanism of Interaction between Functional Groups in the Extraction of Copper (II)	129
	4.15 Comparison of Developed Method for Adsorption of Copper in Real Water	130
Chapter 5	Pollutant Phenol in Water	133
	5.1 Phenolic pollutants	133
	5.2 Phenols	133
	5.2.1 Properties of Phenols	133
	5.2.2 Applications of Phenols	136
	5.3 Effects of Phenol to Human Body and Environment	136
	5.4 Phenol removal methods	137
	5.5 Adsorption of phenol	141
	5.5.1 Adsorbent	142
References		144

LIST OF TABLES

Table 1.1	: Independent variables and their coded and actual values used for optimization
Table 1.2	: Three-factor, three-level central composite design (CCD) used for RSM and its response peak area of chromatogram under different extraction conditions
Table 1.3	: Summary of ANOVA analysis for the extraction procedure
Table 1.4	: Analytical figures of merit of the proposed method for the extraction of phenol
Table 1.5	: Analysis of phenol in environmental water samples
Table 2.1	: The physical properties of the series of amines used in this present research (Liu et al., 2015)
Table 2.2	: The kinetic parameters of the adsorption of phenol by TETA@MNP
Table 2.3	: The adsorption isotherm parameters of phenol by TETA@MNP
Table 2.4	: Comparison of the developed adsorbent with another reported adsorbent
Table 3.1	: Fraction of organic matter in rice husk
Table 3.2	: Physical properties of nanosilica
Table 4.1	: Heavy metal biosorption using various fungal biomass
Table 4.2	: Biosorption of heavy metals using various bacterial biosorbents
Table 4.3	: Biosorption of heavy metals using various algal biosorbents
Table 4.4	: Heavy metal biosorption using various fungal biomass
Table 4.5	: List of Chemicals
Table 4.6	: Parameters for SEM-EDX Analysis
Table 4.7	: Locations of the river water sample collection for each river
Table 4.8	: Characteristics of Azolla through XRD Analysis

Table 4.9	:	Information of calibration curve for copper analyte
Table 4.10	:	Concentration of Copper in Selangor River
Table 4.11	:	Concentration of Copper in Petani River
Table 4.12	:	Concentration of Copper in Langat River
Table 4.13	:	Comparison of adsorbent application in another research
Table 5.1	:	Physical properties of various phenols
Table 5.2	:	Physical properties of phenol
Table 5.3	:	The benefits and drawbacks of various phenol removal methods

LIST OF FIGURES

- Figure 1.1** : Structure of anionic surfactant
- Figure 1.2** : Structure of cationic surfactant
- Figure 1.3** : Structure of zwitterionic surfactant
- Figure 1.4** : Structure of non-ionic surfactant
- Figure 1.5** : TEM image of MNPs
- Figure 1.6** : TEM image of MNP-APTES
- Figure 1.7** : TEM image for MNP-Sylgard 309
- Figure 1.8** : EDX spectra for MNP-Sylgard 309
- Figure 1.9** : EDX spectra for MNP-APTES
- Figure 1.10** : EDX spectra of MNP-Sylgard 309
- Figure 1.11** : FTIR spectra of MNP
- Figure 1.12** : FTIR spectra of MNP-APTES
- Figure 1.13** : FTIR spectra of MNP-Sylgard 309
- Figure 1.14** : XRD pattern of MNP, MNP-APTES and MNP-Sylgard 309
- Figure 1.15** : The magnetization hysteresis loops of MNPs, MNP-APTES and MNP-Sylgard
- Figure 1.16** : The effect of solution pH on the extraction efficiency of phenol
- Figure 1.17** : The effect of adsorbent dosage on the extraction efficiency of phenol
- Figure 1.18** : The effect of desorption solvents on the extraction efficiency of phenol
- Figure 1.19** : The effect of volume of eluent on the extraction efficiency of phenol
- Figure 1.20** : The effect of extraction time on the extraction efficiency of phenol
- Figure 1.21** : The effect of desorption time on the extraction efficiency of phenol
- Figure 1.22** : The effect of sample volume on the extraction efficiency of phenol

- Figure 1.23** : Response surface for the effects of the amount of adsorbent and volume of desorption solvent
- Figure 1.24** : Response surface for the effects of the amount of adsorbent and extraction time
- Figure 1.25** : Response surface for the effects volume of desorption solvent and extraction time
- Figure 1.26** : HPLC-DAD chromatogram (retention time at 2.136s)
- Figure 2.1** : The schematic diagram of the synthesis of amine-functionalized magnetite nanoparticles (EDA@MNP) through chemical co-precipitation
- Figure 2.2** : The FTIR spectra of the synthesized adsorbents
- Figure 2.3** : The SEM micrographs of (A) bare MNPs and (B) EDA@MNP (C) DETA@MNP (D) TETA@MNP (E)TEPA@MNP and (F) PEHA@MNP.
- Figure 2.4** : The EDX spectra of (A) bare MNPs (B)EDA@MNP (C) DETA@MNP (D) TETA@MNP (E) TEPA@MNP, and (F) PEHA@MNP
- Figure 2.5** : The comparison of the percentage removal (%) of the bare MNPs and the series of amine-functionalized magnetite nanoparticles towards phenol adsorption.
- Figure 2.6** : The effect of adsorbent dosage on (A) percentage removal (%) and (B) adsorption capacity (mg/g) of TETA@MNP towards the removal of phenol.
- Figure 2.7** : The effect of contact time on (A) percentage removal (%) and (B) adsorption capacity (mg/g) of TETA@MNP towards the removal of phenol.
- Figure 2.8** : The effect of initial concentration on (A) percentage removal (%) and (B) adsorption capacity (mg/g) of TETA@MNP towards the removal of phenol.
- Figure 2.9** : The effect of pH on (A) percentage removal (%) and (B) adsorption capacity (mg/g) of TETA@MNP towards the removal of phenol.
- Figure 2.10** : (A) The graph of kinetic model pseudo-first-order plot (B) The graph of kinetic model pseudo-second-order plot
- Figure 2.11** : The graphs isotherm models of (A) Freundlich's plot and (B) Langmuir's plot

- Figure 2.12** : The graph of the reusability of TETA@MNP for adsorption of phenol
- Figure 3.1** : Raw rice husk
- Figure 3.2** : Rice husks that are burned and cause high environmental pollution (Mihsen et al., 2017)
- Figure 3.3** : Sequence of rice husk washing process
- Figure 3.4** : The result of combustion deposits from sodium silicate to a white powder of silica
- Figure 3.5** : FTIR silica spectrum
- Figure 3.6** : FTIR silica magnetite nanoparticle spectrum
- Figure 3.7** : XRD spectrum of silica
- Figure 3.8** : XRD spectrum of magnetic silica nanoparticles
- Figure 3.9** : FESEM analysis results of silica
- Figure 3.10** : Results of FESEM analysis of magnetic silica nanoparticles
- Figure 3.11** : TEM analysis results of silica
- Figure 3.12** : Results of TEM analysis of magnetic silica nanoparticles
- Figure 3.13** : EDX spectrum of silica
- Figure 3.14** : EDX spectrum of magnetic silica nanoparticles
- Figure 3.15** : Effect of pH on adsorption of phenol
- Figure 3.16** : Effect of adsorbent mass on adsorption of phenol
- Figure 3.17** : UV-vis graph of absorption against the wave for acetonitrile solvent
- Figure 3.18** : Effect of solvent volume on phenol extraction efficiency
- Figure 3.19** : Effect of extraction time on phenol extraction efficiency
- Figure 3.20** : Effect of adsorption time on phenol extraction efficiency
- Figure 4.1** : (a) Terminalia catappa tree (b) Terminalia catappa fruit (c) Terminalia catappa shell and seed (d) Terminalia catappa Shell Powder in 180 μm
- Figure 4.2** : *Azolla Microphylla Lemna Minor* cultivated in plastic containers
- Figure 4.3** : Overall Methodology Flowchart
- Figure 4.4** : Synthesis technique for the sorbent material

- Figure 4.5** : Photo of a Fourier-transform infrared spectroscopy (FTIR) instrument
- Figure 4.6** : Photo of Scanning Electron Microscope (SEM-EDX)
- Figure 4.7** : Photo of 'Brunanuer-Emmett-Teller' (BET)
- Figure 4.8** : Photo of X-ray Diffraction (XRD)
- Figure 4.9** : Flowchart of heavy metal extraction in water samples.
- Figure 4.10** : The FTIR spectrum of the Azolla adsorbent
- Figure 4.11** : Chemical structure of cellulose
- Figure 4.12** : Chemical Structure of lignin
- Figure 4.13** : SEM micrograph images of the adsorbent material
: at a magnification of 10 Kx with a scale of 10 μm .
(a) Before use (b) After use
- Figure 4.14** : EDX spectrum of Azolla before use.
- Figure 4.15** : EDX spectrum of Azolla after use
- Figure 4.16** : XRD pattern of the synthesized Azolla before the biosorption process
- Figure 4.17** : XRD pattern of the synthesized Azolla after the biosorption process
- Figure 4.18** : Absorption of copper from 10 ppm to 50 ppm using UV-Vis Spectroscopy
- Figure 4.19** : Calibration curve for series of stock solutions of copper from 2 ppm to 10 ppm using UV-Vis Spectroscopy
- Figure 4.20** : Effect of time for the adsorption of copper.
- Figure 4.21** : Effect of adsorbent dosage for the adsorption of copper
- Figure 4.22** : Effect of sample solution pH on the adsorption of copper.
- Figure 4.23** : The spectrum of UV-Vis spectroscopy for the analysis sample in SP3
- Figure 4.24** : The spectrum of UV-Vis spectroscopy for the analysis sample in SL1
- Figure 4.25** : Mechanism of biosorption
- Figure 5.1** : Adsorption process mechanism

ACKNOWLEDGMENTS

With a sincere heart and a wreath of appreciation, we extend our deepest thanks to all the writers who contributed their wisdom, effort, and dedication to the creation of this book. We are profoundly grateful to Universiti Kebangsaan Malaysia (UKM) and the Department of Chemical and Process Engineering, Faculty of Engineering and Built Environment, for affording us the invaluable opportunity to bring this project to fruition.

Our heartfelt gratitude goes to our family members and friends for their unwavering support, patience in sharing our burdens, and encouragement throughout this journey. Your belief in us has been a guiding light. We also wish to acknowledge the contributions of all individuals involved in the success of this endeavour—your efforts, whether directly or indirectly, have been instrumental in bringing this book to life. Thank you to everyone who played a role in this remarkable achievement.

ABSTRACT

The book explores the critical role of magnetite nanoparticles coated with efficient materials as exceptional adsorbents for organic pollutants in water. This book comprehensively delves into the significance of leveraging magnetite nanoparticles in the extraction of pollutants to address the escalating concerns of water pollution worldwide. The research investigates various coating materials and their effectiveness in enhancing the adsorption capabilities of magnetite nanoparticles. The study not only assesses the extraction methods but also evaluates the potential applications of these coated nanoparticles in tackling the pressing issue of water contamination. With a focus on achieving optimal results in pollutant removal, this book provides valuable insights into developing and utilising advanced materials for sustainable water purification.

LIST OF ABBREVIATIONS

AELB	Atomic Energy Licensing Board
IAEA	International Atomic Energy Agency
UKM	Universiti Kebangsaan Malaysia

CHAPTER 1

SYNTHESIS OF MAGNETIC NANOPARTICLES FUNCTIONALIZED WITH SURFACTANT

1.1 Magnetic nanoparticles (MNPs)

Magnetic nanoparticles (MNPs) is a type of nanoparticles that can be manipulated using magnetic fields (Soloveva et al., 2016). An iron atom possesses a robust magnetic moment because of the four unpaired electrons in the 3d shell. Fe^{2+} ions have 4 unpaired electrons in their 3d shell, and Fe^{3+} ions have 5 unpaired electrons in their 3d shell. Thus, the formed crystals from iron ions of Fe^{2+} or Fe^{3+} can be in ferromagnetic or ferrimagnetic states. MNP are vulnerable to air oxidation and can be easily aggregated in aqueous systems (Teymourian et al., 2013). Among the various types of MNPs, magnetite (Fe_3O_4) is commonly studied due to its advantages, such as superior high surface area, low toxicity, small particle size, ease of dispersion in water and high magnetic properties (Bui et al., 2018)

Magnetic field-based separation using magnetic nano and microparticles has received significant attention for their superior characteristics, such as good dispersion, rapid and effective binding of targets and reversible and controllable flocculation (Su et al., 2015). Due to the large surface area, MNPs guarantee high extraction efficiency when dealing with small sample volumes (Karimi et al., 2016).

The main issue in applying MNPs in these fields is their chemical stability and level of dispersion in the solution. Due to van der Waals forces and high surface energy, these nanoparticles tend to agglomerate easily in an aqueous medium due to van der Waals forces (Laurent et al., 2008). In addition, they are highly reactive and susceptible to oxidation by air, resulting in a loss in magnetism and dispersibility (Shahrman et al., 2018).

These problems can be solved by surface modification of MNPs with appropriate organic coating. Recently, organic compounds such as silane, octadecylsilane, triphenylamine and polymers are often used to coat the surface of MNPs to maintain their chemical stability in various media.

Among these, silicone non-ionic surfactants are potential modification agents for MNPs. Using this surfactant as a coating agent aids in obtaining the desired colloidal dispersion, which also provides a large surface area, high stability, and applicability in harsh chemical media.

For many applications, surface modification of MNPs is a crucial challenge. MNP, with some surface modifications, can be used to separate and concentrate chemicals conveniently using an external magnetic field. Therefore, integrating magnetic separation and surface modification would provide a powerful analytical tool with simplicity, flexibility and selectivity (Su et al., 2015).

1.2 Surfactants

1.2.1 Properties of Surfactants

Surfactants are organic compounds of polar head and non-polar tail groups in natural and synthetic forms. They form self- assembled aggregates like micelles in the presence of water. Surfactants are added as wetting agents to lower the liquids' surface tension. They are also used to spread and lower the interfacial tension of the liquids readily.

The surfactants' polar head and non-polar tail are always organic compounds which contain hydrophilic and hydrophobic groups, respectively. Hydrophilic molecules comprise ions like sulphate and carboxylate from polar groups such as primary amines, amine oxides, and non-polar groups, with electronegative atoms like oxygen atoms and aldehydes or amides. The hydrophilic group gives solubility characteristics in polar solvents, while the hydrophobic group enhances solubility characteristics in non-polar solvents such as oil. The hydrophilic and hydrophobic determine the size and shape of surfactants (Nkadi et al., 2009). Surfactants can be classified using charged groups in their head. Four groups in surfactants are anionic, cationic, zwitterionic and non-ionic.

1.2.2 Types of Surfactants

1.2.2.1 Anionic Surfactants

The anionic surfactant contains a negatively charged head group. The negative charge causes repelling because of the slightly negative surface. High amounts of anionic surfactant are causing foaming in the solution. An example of an anionic surfactant is sodium lauryl sulphate, which has high

solubility in water at room temperature (Johansson & Somasundaran, 2007). Their water solubility depends on the double bond of the structure. They are stable under a pH of more than 10 and sensitive to acids. Figure 1.1 shows the structure of anionic surfactant, which contains a hydrophilic head (negative charge head group) and a long hydrophobic tail.

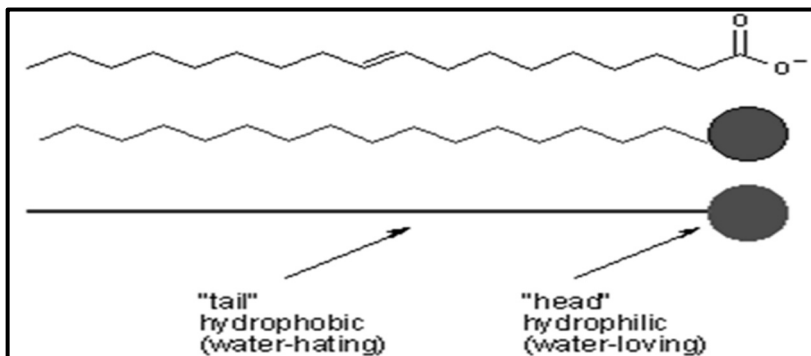


Figure 1.1 Structure of anionic surfactant

Source: Formulation of Carpet Cleaners. In Handbook for Cleaning/Decontamination of Surfaces

Anionic surfactant is widely used in pharmaceutical and cosmetic applications. They are usually used in cleaning applications. For example, they have been used to emulsify oily soils and lift soils from surfaces (Johansson & Somasundaran, 2007). In addition, they are also one of the ingredients in shampoo used for cleaning and hair conditioning. Moreover, oil removal also could be achieved by using this surfactant. Typical anionic surfactants are alkyl sulphates, alkyl ethoxylate sulphates, soaps, carboxylate, sulfate and sulfonate ions.

1.2.2.2 Cationic surfactants

Cationic surfactant is a positively charged head group surfactant (Gelardi et al., 2016). They are hydrophilic, which is water-loving and contain positively charged ions. Examples of cationic surfactants include trimethyl alkylammonium chlorides and the chlorides or bromides of benzalkonium and alkyipyridinium ions. They are quarternary ammonium compounds and good as emulsifying agents and do not form insoluble scums. Figure 1.2 shows the cationic surfactant structure with a positively charged group in its head.

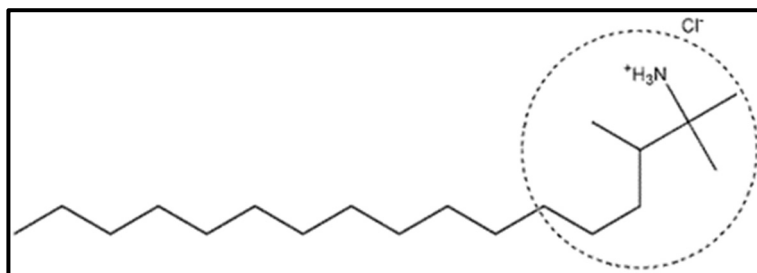


Figure 1.2 Structure of cationic surfactant

Cationic surfactants are widely used in applications involving preservation and disinfection from bacteria. They are good bactericides and can be used as antiseptics to clean wounds or burns. They have bactericidal activity against some positive or negative organisms, so they are heavily used in bathrooms and hand sanitisers. Cationic surfactants such as quaternary ammonium and pyridinium are essential for pharmaceutical use (Tadros, 2009).

1.2.2.3 Zwitterionic surfactants

Zwitterionics is a mild surfactant. They can be present as anionic (negatively charged), cationic (positively charged) or non-ionic (no charge) in solution, which depends on the pH of the water. They contain groups of two different charges. The positive charge group is ammonium, while the negative is carboxylate or sulphate. Figure 1.3 shows the zwitterionic surfactant structure containing the same group's negative charge and positive charge.

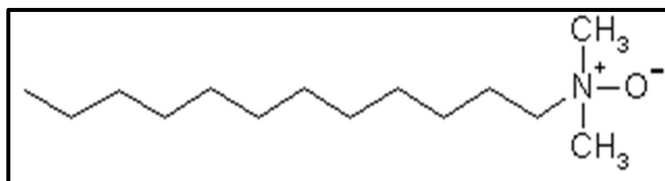


Figure 1.3 Structure of zwitterionic surfactant

This type of surfactant is widely used in personal care products for sensitive skin. This surfactant has effective dermatological properties and is commonly used in shampoos, detergents and other cosmetic products (Fernley, 1978).

1.2.2.4 Non-ionic surfactants

Non-ionic surfactants are known as derivatives of ethylene oxide and/or propylene oxide with an alcohol which contains an active hydrogen atom. Non-ionic surfactants do not have positive or negative charges on their head groups (Sonia & Sharma, 2014), preventing them from dissolving in the aqueous solution group (Figure 1.4). Examples of non-ionic surfactants are polyglycerol alkyl ethers, glucosyl dialkyl ethers, and crown ethers.

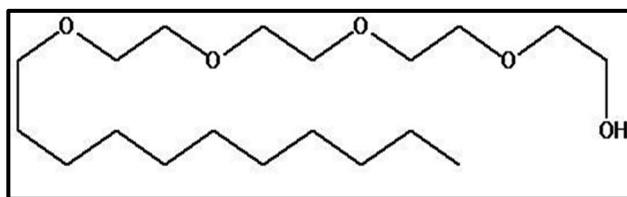


Figure 1.4 Structure of non-ionic surfactant

This non-ionic surfactant is very difficult to maintain and create the emulsion so it is known as emulsifying agent (Zhang et al., 2012). They can effectively remove oil and emulsifiers. They are widely used in industry as they are low cost, biodegradable, high chemical stability (Manosroi et al., 2003) and less irritant than other surfactant (Sonia & Sharma, 2014). These unique properties allow surfactants to be a potential coating agent for modifying MNPs' surfaces. The combination of magnetic properties of MNPs with surfactant offers the development of a new adsorbent with high chemical stability and efficiency.

1.3 Surfactant-modified magnetic nanoparticles

Recently, researchers have succeeded in developing nano-composites of MNPs and surfactants to separate organic contaminants in real matrices. Muthukumaran et al. (2016) have synthesized sodium dodecyl sulphate (SDS) coated MNPs as an effective, low-cost adsorbent for removal of cationic dye, crystal violet (CV) from aqueous solution. They found that SDS-coated MNPs are cost-effective and easily separable nano-adsorbents for efficiently removing crystal violet dye. They also studied adsorption isotherms and kinetic parameters of crystal violet dye removal from aqueous solution using this surfactant-modified magnetic nano-adsorbent.

Li et al. (2008) have introduced cetyltrimethylammonium bromide (CTAB)-coated Fe_3O_4 nano-magnets (CTAB-coated Fe_3O_4 NP) for enrichment of

selected chlorophenols in aqueous matrices before HPLC –UV determination. The fabricated CTAB-coated Fe_3O_4 NP combined with mixed hemimicelles SPE technique showed good recoveries and precision, revealing that the proposed method based on CTAB-coated Fe_3O_4 NP has potential for preconcentration of trace organic pollutants from environmental water samples. Another study by Zhao et al. (2008) also reported the preparation of cation surfactants, cetyltrimethylammonium bromide (CTAB) and cetylpyridinium chloride (CPC) onto magnetic nanoparticles for mixed hemimicelles solid-phase extraction (SPE) method to separate several phenolic compounds including bisphenol A (BPA), 4-tert-octylphenol (4-OP), and 4-n-nonylphenol (4-NP) from real aqueous matrices. It was found that the proposed adsorbents CTAB and CPC modified on Fe_3O_4 nanoparticles (Fe_3O_4 NPs) have strong electrostatic and hydrophobic interactions with studied analytes. The proposed method provided some advantages such as high recoveries, high breakthrough volumes and short separation times.

All the studies regarding the applications of the ionic surfactants modified magnetic nanoparticles towards hazardous contaminants demonstrate that the nanocomposites are effective adsorbents for treating and determining these pollutants. In this study, silicone non-ionic surfactant Sylgard 309 is used to functionalize the surface of MNPs because it has flexible polysiloxane chains without any aromatic structure, which is advantageous compared to other frequently used non-ionic surfactants, namely Triton X, Tergitol and PONPE series as none of them considered suit with HPLC-DAD, where Diode Array HPLC Detectors are most commonly used to record the ultraviolet and visible (UV-vis) absorption spectra of samples that are passing through high-performance liquid chromatography. This is due to their aromatic chromophore, which has strong UV absorbance or fluorescence signals that become obstacles for UV and fluorescent detectors. The current research focused on using silicone non-ionic surfactant Sylgard 309 modified MNPs for magnetic solid phase extraction of phenols from environmental water matrices before HPLC-DAD analysis. To our knowledge, no studies have investigated this idea yet.

1.3.1 Synthesis of MNP with ferum oxide and surfactant Slygard

MNPs were synthesized using the wet chemical coprecipitation method. A 3.1736 g of $\text{FeCl}_2 \cdot 4\text{H}_2\text{O}$ and 7.5684 g of $\text{FeCl}_3 \cdot 6\text{H}_2\text{O}$ were dissolved in 320 ml of deionized water, such that $\text{Fe}^{2+}/\text{Fe}^{3+} = 1/2$. The mixed solutions were

stirred under N_2 at 80 °C for 1 hour. Then, 40 ml of NH_3H_2O was injected into the mixture rapidly, stirred under N_2 for another hour and cooled to room temperature. The precipitated particles were washed five times with hot water and separated by magnetic decantation. Finally, magnetic nanoparticles were dried under a vacuum at 70 °C.

4.2252 g Fe_3O_4 MNPs was sonicated in 150 mL of ethanol/water (volume ratio, 1:1) solution for 30 minutes to obtain uniform dispersion. Then 16.1600 g (17 mL) of APTES was added to the solution under N_2 atmosphere at 40 °C for 2 hours. The optimal surface modification in a molar ratio of APTES to Fe_3O_4 was found at 4:1. After that, the solutions were cooled at room temperature. The prepared APTES-modified Fe_3O_4 MNPs were separated with a magnet and washed with ethanol, followed by deionized water three times. Finally, APTES-modified Fe_3O_4 (Fe_3O_4 -APTES) were dried under vacuum at 70°C.

0.2000 g of Fe_3O_4 -APTES MNPs was dispersed in 8.0000 g of 3-(3-Hydroxypropyl)–Heptanethyltrisiloxane (Sylgard 309) non-ionic surfactant solution with continuous stirring overnight at room temperature under N_2 gas. The suspension was then washed with ethanol three times. The precipitated particles were collected by magnetic decantation. Finally (Fe_3O_4 -APTES-Sylgard 309) was dried under vacuum at 70°C.

1.4 Characterization of MNP with ferum oxide and surfactant Sylgard

The magnetic nanoparticles (MNPs) combined with surfactant Slygard were firstly characterized for the functional groups by an FTIR spectrometer (Thermo Nicolet, Nexus 670) in the absorption mode with 32 scans and a resolution of $\pm 4\text{ cm}^{-1}$, a wave-number range of 4000–400 cm^{-1} . For the KBr pellet technique, optical grade KBr was used as the background material. The MNPs were intimately mixed with dried KBr at the ratio of MNPs: KBr = 1:100, then compressed into pellets under pressure.

A wide-angle X-ray diffractometer (Bruker D8 Advance) was used to study the crystalline structure of the synthesized MNPs below the nanometer scale. The CuK-alpha radiation source was operated at 40 kV/30 mA. The MNPs were placed into a sample holder, and the measurement was continuously run. The experiment was recorded by monitoring the diffraction pattern in the 2 θ range from 10 to 80 with a scan speed of 1°/min and a scan step of 0.02°.

A transmitting electron microscope (FEI Talos L120C, resolution of 0.2nm@120kV) was used to examine the morphological structure and to measure the particle size of the MNPs. The samples were placed on the holder with adhesive tape and coated with a thin layer of platinum using an ion sputtering device for 1 min prior to observation under SEM. The SEM images were obtained using the acceleration voltage of 5 kV with a magnification of 100-150 kx. The average particle sizes are determined by randomly capturing SEM images from 500 nanoparticles.

Energy dispersive X-ray (EDX) was used for the elemental analysis or chemical characterization of a sample.

A vibrating sample magnetometer (VSM) Lakeshore 7404 Series was used to study the magnetic properties of the MNPs. The hysteresis loops were measured under a magnetic field strength of 10,000 Gauss at room temperature. The data were taken with 80 points/loop and a 10 s/ point scan speed.

1.4.1 Morphological analysis

The particle size of MNPs, MNP-APTES and MNP-Sylgard 309 were investigated using TEM, as shown in Figure 1.5, Figure 1.6 and Figure 1.7. The prepared nanoparticles with an approximate spherical shape and uniform nano-size distribution were observed. From the diameter distribution (Figures 1.6, 1.7, 1.8), it could be seen that the average diameters of MNPs, MNP@APTES, and MNP-Sylgard 309 are increases which can be related to encapsulation of APTES and surfactant Sylgard 309, respectively onto the surface of MNPs.

In addition, the TEM image of MNPs showed that they were agglomerated due to large specific surface area and high surface energy. After being coated with APTES, the MNP-APTES particles are well dispersed, as APTES prevent the interparticle interactions between MNPs particles. After introducing surfactant Sylgard 309, the dispersion of the MNP-Sylgard 309 nanoparticles was enhanced because surfactant Sylgard 309 provided sufficient repulsive interactions between nanoparticles, reducing the agglomeration between the MNPs particles.

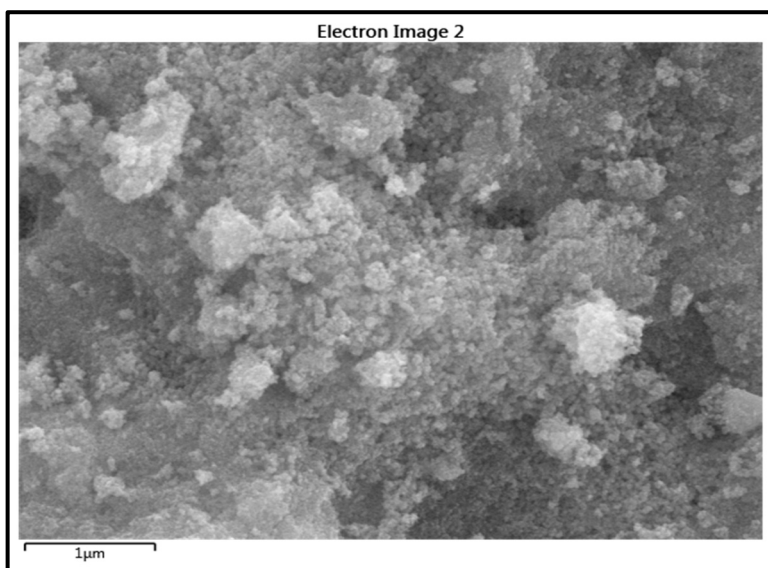


Figure 1.5 TEM image of MNPs

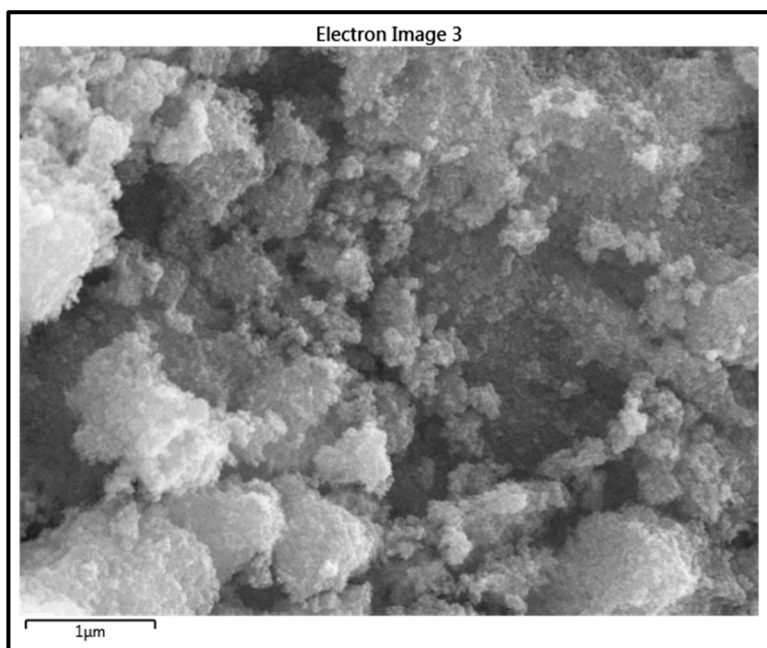


Figure 1.6 TEM image of MNP-APTES

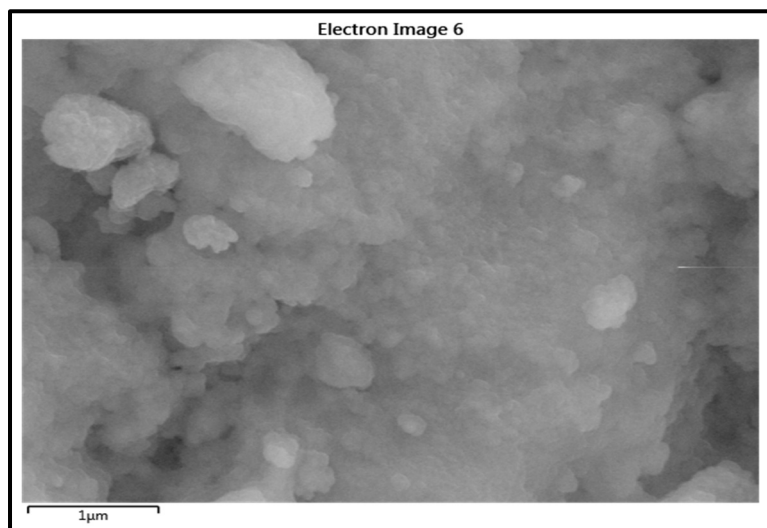


Figure 1.7 TEM image for MNP-Sylgard 309

1.4.2 Elemental analysis

EDX analysis was performed to provide elemental identification and quantitative compositional information elements such as N, O, Fe, Si, and C in the prepared MNPs, MNP-APTES and MNP-Sylgard 309 (Figure 1.8, Figure 1.9 and Figure 1.10). The elemental analysis of the MNPs sample showed that MNPs only contain 71.2% Fe and 25.6% O. After the modification with APTES, the presence of new elements, such as 4.0% C and 1.2% Si, confirmed the APTES was successfully anchored to the surface of MNPs. Finally, as evident from the spectrum of MNP-Sylgard 309, the high percentage of C (17.1%), Si (3.1%) and O (26.1%) in MNP-Sylgard 309 revealed that the surfactant Sylgard 309 was successfully introduced onto the surface of MNP-APTES.

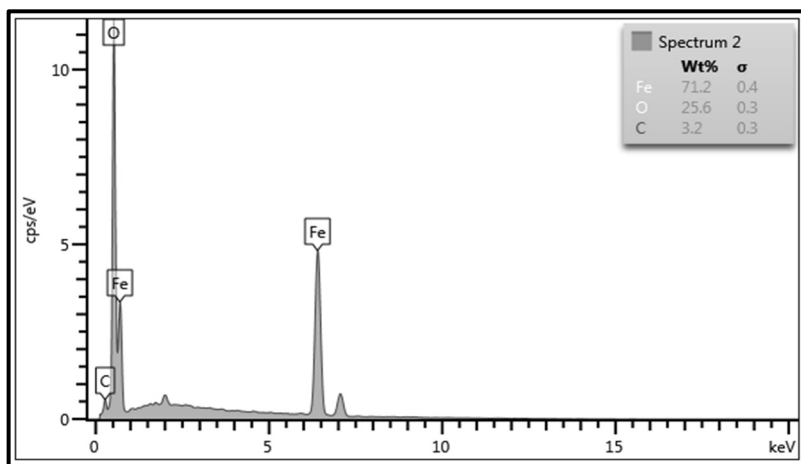


Figure 1.8 EDX spectra MNP

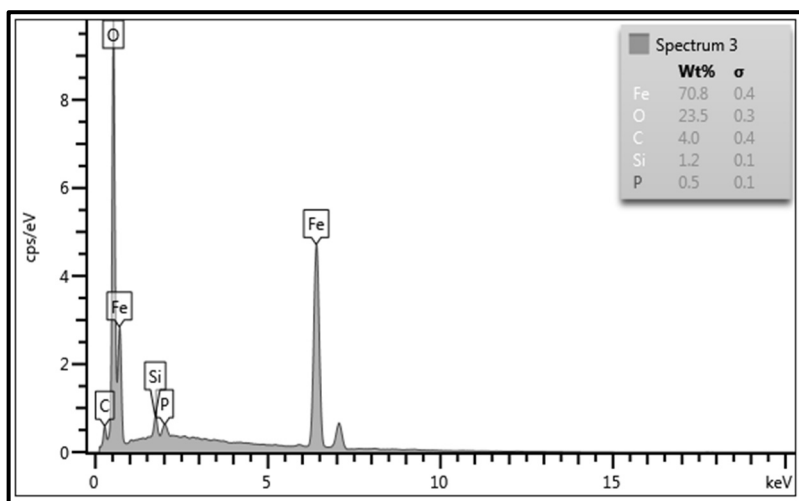


Figure 1.9 EDX spectra of MNP-APTES

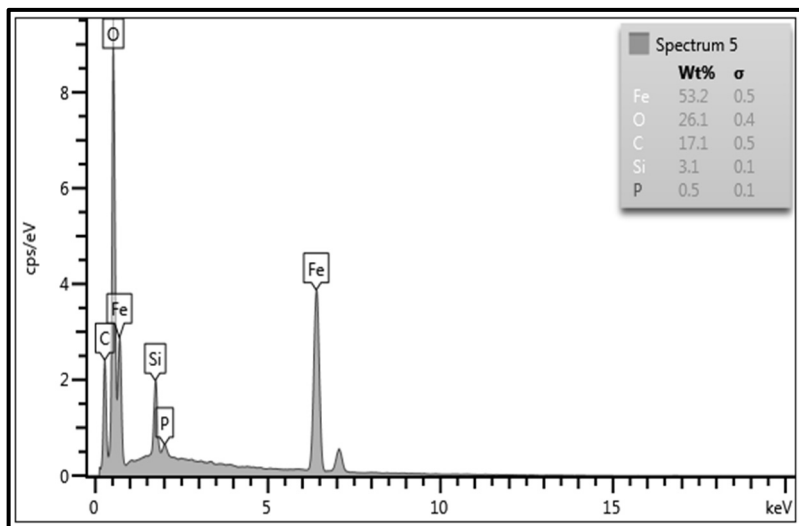


Figure 1.10 EDX spectra of MNP-Sylgard 309